BIOCHEMISTRY
including biophysical chemistry & molecular biology

Article

pubs.acs.org/biochemistry

The Semiquinone at the Q_i Site of the bc_1 Complex Explored Using HYSCORE Spectroscopy and Specific Isotopic Labeling of Ubiquinone in *Rhodobacter sphaeroides* via ^{13}C Methionine and Construction of a Methionine Auxotroph

Sangjin Hong,[†] Wagner B. de Almeida,[‡,#] Alexander T. Taguchi,[§] Rimma I. Samoilova,[∥] Robert B. Gennis,[†] Patrick J. O'Malley,*[,‡] Sergei A. Dikanov,*[,⊥] and Antony R. Crofts*[,†]

[†]Department of Biochemistry, University of Illinois at Urbana-Champaign, Urbana, Illinois 61801, United States

[‡]School of Chemistry, The University of Manchester, Manchester M13 9PL, U.K.

[§]Center for Biophysics and Computational Biology, University of Illinois at Urbana-Champaign, Urbana, Illinois 61801, United States

[∥]V. V. Voevodsky Institute of Chemical Kinetics and Combustion, Russian Academy of Sciences, Novosibirsk 630090, Russian Federation

[⊥]Department of Veterinary Clinical Medicine, University of Illinois at Urbana-Champaign, Urbana, Illinois 61801, United States

Supporting Information

ABSTRACT: Specific isotopic labeling at the residue or substituent level extends the scope of different spectroscopic approaches to the atomistic level. Here we describe ^{13}C isotopic labeling of the methyl and methoxy ring substituents of ubiquinone, achieved through construction of a methionine auxotroph in *Rhodobacter sphaeroides* strain BC17 supplemented with L-methionine with the side chain methyl group ^{13}C-labeled. Two-dimensional electron spin echo envelope modulation (HYSCORE) was applied to study the ^{13}C methyl and methoxy hyperfine couplings in the semiquinone generated *in situ* at the Q_i site of the bc_1 complex in its membrane environment. The data were used to characterize the distribution of unpaired spin density and the conformations of the methoxy substituents based on density functional theory calculations of ^{13}C hyperfine tensors in the semiquinone of the geometry-optimized X-ray structure of the bc_1 complex (Protein Data Bank entry 1PP9) with the highest available resolution. Comparison with other proteins indicates individual orientations of the methoxy groups in each particular case are always different from the methoxy conformations in the anion radical prepared in a frozen alcohol solution. The protocol used in the generation of the methionine auxotroph is more generally applicable and, because it introduces a gene deletion using a suicide plasmid, can be applied repeatedly.

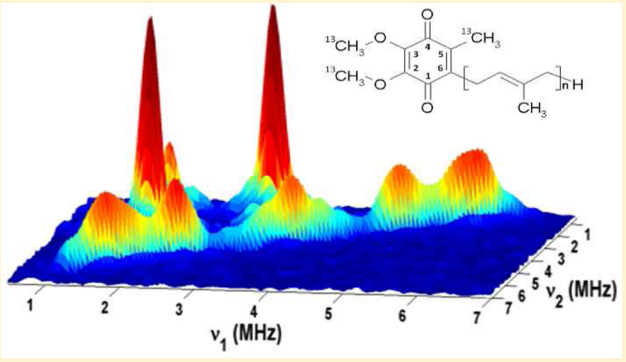

The biosphere is driven by membrane proteins that participate in protonic circuits in which redox or photoredox reactions drive the generation of the proton gradient used to sustain the cell through a variety of direct and indirect pumps and nanomachines.[1−3] As structures have become available, and as molecular engineering approaches have facilitated direct tests of the structural underpinnings, our understanding of mechanism has expanded from the "black-box" view provided by simple physicochemical approaches to the molecular level. Advances in spectroscopy have supplemented this broad front to provide atomistic detail. These methods can be amplified by specific isotopic labeling. However, the enzymes of interest are often studied in a context where such labeling is not available. Specific labeling requires the use of auxotrophic strains and in the past has entailed expression of the protein of interest in a prokaryotic background in which auxotrophic strains have been developed, most commonly in *Escherichia coli* (cf. refs 4 and 5) The photosynthetic bacterium *Rhodobacter sphaeroides* has become a test vehicle for mechanistic studies of a number of respiratory and photosynthetic membrane proteins. Under different growth conditions, it expresses a remarkable metabolic versatility, for example, a "mitochondrial" respiratory chain under aerobic conditions and a photosynthetic chain under anaerobic illumination. Because for many of the enzymes of interest the functional complex cannot be expressed in *E. coli*, it has not been possible to take advantage of specific isotopic labeling except by *in vitro* substitution. Auxotrophic strains have been

Received: May 28, 2014
Revised: September 2, 2014
Published: September 3, 2014

   dx.doi.org/10.1021/bi500654y | *Biochemistry* 2014, 53, 6022−6031

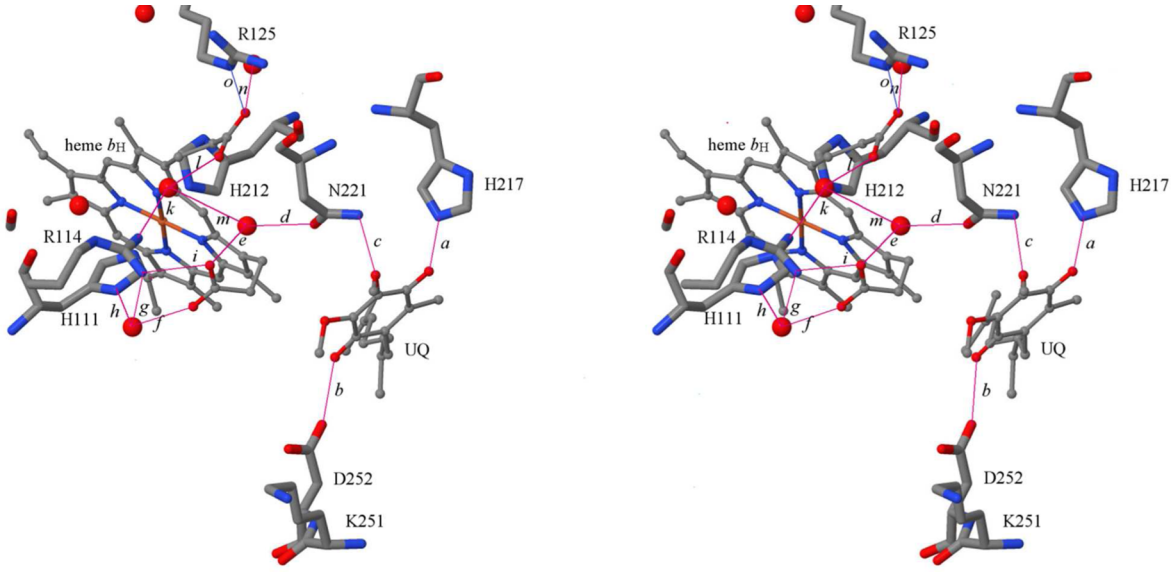

Figure 1. Q_i site topology. Liganding of ubiquinone at the Q_i site of the *Rb. sphaeroides* bc_1 complex, showing potential hydrogen bonding partners. Also shown is the network of hydrogen bonds connecting Asn-221 and other residues to the heme b_H propionates and His-111, one of the heme Fe ligands. The stereopair is for crossed-eye viewing: structural data from PDB entry 2QJY, chain D. Residues discussed herein are shown as wireframe models, labeled by residue number; UQ and heme b_H are shown as ball-and-stick models, and crystallographic waters are represented by spheres showing their O atoms (atom coloring is CPK). Bonds of interest are shown as magenta lines, labeled by lowercase italic letters, with details in Table 1. The hydrogen bond network involving crystallographically defined waters (bonds *d*–*m*) is discussed in the text.

developed in *Rb. sphaeroides* by MacKenzie and colleagues,[6] but in the wild-type 2.4.1 background, where they were generated by transposon mutagenesis, which is a random technique. Most studies of particular enzymes are performed in a modified genetic background specifically developed to facilitate mutagenesis, protein purification, deletion of extraneous genes for functions that interfere with measurement, etc., and in these cases, it is of interest to generate auxotrophic strains by deletion of a particular gene. Here we demonstrate a general method for achieving this end through construction of a methionine auxotroph in *Rb. sphaeroides*.

Central to all the major electron transfer chains are enzymes of the cytochrome (cyt) bc_1 complex family,[7−9] which under many physiological conditions control the flux. In the mitochondria that power eukaryotic cells, the cyt bc_1 complex is known as complex III of the respiratory chain, but the simpler enzymes of bacteria perform the same enzymatic function and are more accessible to the experimental spectroscopic and kinetic approaches exploited in previous work.

The Q cycle mechanism of the cyt bc_1 complex[8,10−13] results in oxidation of two quinol (QH_2) molecules with release of four protons to the positive side of the membrane (P phase, the intermembrane space in mitochondria, the periplasm of bacteria), reduction of one quinone (Q) with uptake of two protons from the negative side (N phase, the matrix in mitochondria, the cytoplasm in bacteria), and the transfer of two electrons between these phases, in an overall reaction for turnover given by

$$QH_2 + 2\text{ferricyt } c + 2H^+_N \rightleftharpoons Q + 2\text{ferrocyt } c + 4H^+_P \quad (1)$$

In the forward chemistry of the Q cycle, electrons from the intermediate semiquinone generated at the Q_o site (SQ_o) upon oxidation of QH_2 are delivered to the Q_i site by the low-potential chain (hemes b_L and b_H) to reduce Q to QH_2 in a two-electron gate mechanism.[13] With the quinone pool initially oxidized, the electron from the first turnover of the Q_o site (using QH_2 generated in the photochemistry) crosses the membrane to reduce Q at the Q_i site to SQ_i, while that from the second turnover reduces SQ_i to QH_2. The SQ_i intermediate at the Q_i site (SQ_i) is relatively stable[14,15] and can be generated by forward chemistry, by reversal of the second step upon addition of a reductant (ascorbate or QH_2) to the complex with heme b_H oxidized, or by redox titration. The physical chemistry of the reaction can be studied via the kinetics of electron transfer using spectrophotometry of the heme centers, and the thermodynamics by taking advantage of the paramagnetic properties of the SQ_i. The redox potentials of the SQ_i couples can be gleaned from the bell-shaped titration curve, which when studied as a function of pH also maps out p*K* values important for the mechanism.[14,15] Current controversies discuss how these mechanistic considerations relate to structures and atomistic detail. Several structures show a quinone species bound at the Q_i site; that from Protein Data Bank (PDB) entry 2QJY[16] shows the *Rb. sphaeroides* structure, which is most pertinent to this study (Figure 1). Specific mutagenesis coupled with kinetic, spectroscopic, and thermodynamic measurements to explore functional consequences had indicated that the three potential H-bonding partners shown in Figure 1 were all important.[10,17−19] More recently, high-resolution EPR approaches have been used to explore the interaction between the SQ_i paramagnet and nuclear spins in the immediate environment.[20−24] Our own results were quite coherent with the mutagenesis studies and the structure shown; they revealed spin interaction with a N atom, with characteristics compatible with the direct H-bond to N_ε of His-217 of the cyt *b* subunit, additional ^1H or ^2H interactions indicating a second H-bond, likely to either a water or Asp-252, and no other strong spin interaction with protein or solvent.[20−22] However, structural interpretations from both crystallographic[25−30] and spectroscopic approaches[23] have been

dx.doi.org/10.1021/bi500654y | *Biochemistry* 2014, 53, 6022−6031

controversial, with several other suggestions for H-bonding partnerships.

Table 1. Parameters for Bonds Shown in Figure 1

label	bond distance (Å)	atom 1	atom 2
a	2.26	H217 NE2	UQ2 O4
b	4.78	D252 OD2	UQ2 O1
c	4.56	N221 ND2	UQ2 O3
d	2.73	N221 OD1	H_2O 1163
e	2.51	H_2O 1163	heme O2A
f	2.59	H_2O 1161	heme O1A
g	3.35	R114 NH1	H_2O 1161
h	2.85	H111 ND	H_2O 1161
i	3.13	R114 NH2	heme O2A
k	3.5	R114 NH2	H_2O 1162
l	2.47	heme O1D	H_2O 1162
m	3.64	H_2O 1162	H_2O 1163
n	2.64	heme O2D	H_2O 1115
o	2.67	R125 NE	heme O2D

Bond *a* is the primary bond stabilizing Q. Bond *b* is likely an indirect H-bond through water, as seen in some structures. Bond *c* is included to show distance, but no evidence for bond. The set of H-bonds *d* through *o* connects the heme ligand, His-111, and the heme propionates, to crystallographically defined waters and the protein, to form a network. It seems likely that this network is more extensive and links to proton conduction pathways to the aqueous phase through which protons equilibrate with the heme, and possibly with changes in redox state of the quinone, during the Q_i-site reaction.

Detailed information about the influence of the protein environment on the electronic structure and distribution of the unpaired spin density can be obtained from analysis of ^{13}C couplings of carbon nuclei in the quinone ring and substituents.[5,31] However, as noted above, these data are currently not available for the SQ_i in the Q_i site, because approaches for selective isotopic labeling of proteins and cofactors have not been developed in *Rb. sphaeroides*. In this work, we demonstrate isotopic labeling of the ring substituents of ubiquinone, achieved through construction of a methionine auxotroph in *Rb. sphaeroides* strain BC17. We extend our studies by ^{13}C labeling of the methyl and methoxy substituents of the ubiquinone ring using ^{13}C-labeled L-methionine, which in the synthetic pathway provides the methyl groups. ^{13}C hyperfine couplings for the methyl and two methoxy groups of SQ_i generated *in situ* in the native complex in its membrane environment were determined by 2D ESEEM (HYSCORE). Analysis of the data with the aid of DFT calculations has provided a first look at the distribution of the unpaired spin density over the ring and conformations of methoxy groups in SQ_i.

EXPERIMENTAL PROCEDURES

Construction of the Methionine Authotroph of *Rb. sphaeroides*. A methionine (Met) auxotroph of *Rb. sphaeroides* was generated by replacing the *metA* gene in the chromosome with a *cat* gene that provides chloramphenicol resistance. For the generation of the auxotroph, the chloramphenicol resistance cassette flanked by ~500 bp regions homologous to the upstream and downstream regions of *metA* was constructed by three-step polymerase chain reactions (PCRs). The double-stranded linear PCR product was then inserted into suicide vector pLO1 containing the *sacB* gene that kills Gram-negative cells when expressed in the presence of sucrose.[32,33] The recombinant pLO1 derivative was transformed into *E. coli* S-17 and then mobilized into *Rb. sphaeroides* BC17, a bc_1-deficient strain,[34] by biparental conjugation.[35] The *Rb. sphaeroides* conjugants were selected by their newly acquired chloramphenicol resistance, and the cells containing the pLO1 derivatives among the conjugants were deselected by culture in the presence of sucrose. The deletion of *metA* in the finally selected strains (*metA*::*cat*) was verified by the Met auxotrophic phenotype. Growth of this strain in the presence of ^{13}C methylmethionine results in ^{13}C labeling of the methoxy and methyl carbons of the substituents at positions 2, 3, and 5 on the ring of ubiquinone-10 (UQ-10) (Scheme 1). Strain BC17

Scheme 1

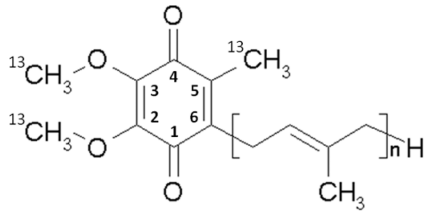

was derived from strain Ga, in which the carotenoid synthetic chain of the parental 2.4.1 wild type was truncated by random mutagenesis. In the BC17 strain, the *fbc* operon encoding the bc_1 complex was deleted from the chromosome to generate a background for experiments in which expression of the catalytic subunits of the bc_1 complex from the plasmid-borne operon in strains with specific mutations has been exploited in the exploration of details of the mechanism. This library of mutant strains from previous work is now available for further study using isotopic labeling.

Preparation of Chromatophores. Chromatophores were prepared according to established methods.[36] Chromatophores are sealed vesicles formed upon mechanical disruption of cells; inner membrane invaginations break off and reseal, and they contain the periplasmic medium (including cyt c_2) and the entire membrane-bound apparatus for photosynthetic phosphorylation. The bc_1 complex is therefore in its native state and reacts with its native partners. The composition of the chromatophore membrane depends on growth conditions, strain, etc., and can vary quite substantially. In the Ga parental strain, when cells are grown under standard laboratory conditions and harvested in late log phase, the ratio of bacterial reaction center to bc_1 complex is approximately 2:1; however, the components are likely distributed at random, and the ratio in individual vesicles is stochastic within normal limits. However, the mean ratio can vary over a wide range.[37]

Characterization of the Q_i Site Semiquinone. Redox titrations were performed in a potentiometric cell maintained under anaerobic conditions using argon gas. Chromatophores were suspended in 100 mM KCl and 50 mM MOPS (pH 7.0) or 100 mM KCl and 50 mM CHES (pH 9.2) to a reaction center concentration of ~0.7 mM, and the redox potential was adjusted by adding small aliquots of potassium ferricyanide or sodium dithionite. The following redox mediators were present: 4 μM each of 2-OH-1,4-naphthoquinone and pyocyanin; 8 μM each of 3,6-diaminodurene, phenazine ethosulfate, and

dx.doi.org/10.1021/bi500654y | *Biochemistry* 2014, 53, 6022−6031

phenazine methosulfate; and 40 μM each of *p*-benzoquinone, 1,2-naphthoquinone, 1,4-naphthoquinone, and duroquinone. The samples were taken in the dark at the desired E_h values using an airtight syringe, placed in argon-flushed EPR tubes, frozen rapidly, and stored in liquid nitrogen until the samples were measured. At each point shown in the titration, data were obtained in the absence and presence of antimycin, and the value shown represents the difference, giving the antimycin-sensitive component (see Figure S1 of the Supporting Information and its legend), contributing ~87% of the overall signal at the peak of the curve. However, because the antimycin-insensitive component showed essentially the same amplitude over the range of the titration, the fractional contributions varied.

EPR and ESEEM Measurements. The CW EPR measurements were performed on an X-band Varian EPR-E122 spectrometer, with the sample at 100 K. The pulsed EPR experiments were conducted using an X-band Bruker ELEXSYS E580 spectrometer equipped with an Oxford CF 935 cryostat. All pulsed EPR measurements were taken at 80 K. The 2D ESEEM, four-pulse experiment ($\pi/2-\tau-\pi/2-t_1-\pi-t_2-\pi/2-\tau-$echo, also called HYSCORE), with a magnetic field of 343.0 mT, a time between the first and second pulses (τ) of 136 ns, and a microwave frequency of 9.619 GHz,[38] was employed with appropriate phase cycling schemes to eliminate unwanted features from the experimental echo envelopes. The intensity of the echo after the fourth pulse was measured with t_2 and t_1 varied and a constant τ. The length of a $\pi/2$ pulse was 16 ns and that of a π pulse 32 ns. HYSCORE data were collected in the form of 2D time domain patterns containing 256 × 256 points with steps of 20 or 32 ns. Spectral processing of ESEEM patterns, including subtraction of the relaxation decay (fitting by polynomials of three to six degrees), apodization (Hamming window), zero filling, and fast Fourier transformation (FT), were performed using Bruker WIN-EPR version 2.22 revision 10. Processed data were then imported into Matlab R2010a via the EasySpin package[39] either to be simulated by EasySpin version 4.5.5 or to be analyzed by a homemade script for fitting data in $(\nu_1)^2$ versus $(\nu_2)^2$ coordinates. After the HYSCORE had been plotted as $(\nu_1)^2$ versus $(\nu_2)^2$, ridges were fit via a linear regression with each point on the ridge weighted according to its HYSCORE intensity (see below). The peculiarities of powder ^{13}C HYSCORE spectra and all details of the analysis of the ^{13}C cross-peaks from methyl and methoxy substituents are described in the recent study of the ^{13}C-labeled SQs in the Q_A and Q_B sites of the bacterial reaction center (see also the Supporting Information).[31]

Computational Methods. All density functional calculations were performed using Gaussian 09.[40] Geometries were partially optimized at the B3LYP/6-31G(d) level, and hyperfine couplings were calculated at the B3LYP/EPR-II level.

RESULTS

Physicochemical Properties of the Q_i Site Semiquinone. The antimycin-sensitive semiquinone generated in this work was similar to those reported earlier in chromatophores from *Rb. sphaeroides*[15] or in submitochondrial particles[14] (Figure 2). The two values of pH at which measurements were taken preclude detailed discussion of E_m–pH relationships, but our results are consistent with the previous work. The ^{13}C labeling of the methyl groups does not influence the SQ line width, indicating that it is still dominated by the **g**-tensor anisotropy, and likely in the anionic form. The

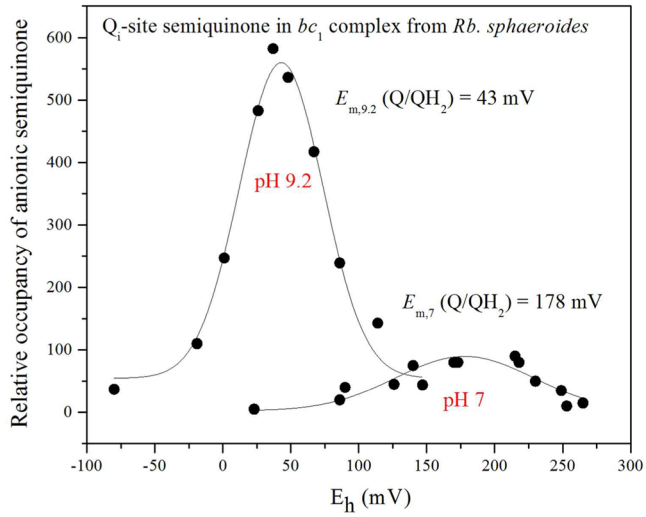

Figure 2. Potentiometric titration curves of the SQ_i EPR signals at pH 7.0 and 9.2. The spectra were obtained in the range of redox potentials between −80 and 265 mV vs the standard hydrogen electrode (SHE). Redox potentiometry was performed under argon with redox mediators, and the semiquinone radical was titrated with sodium dithionite. EPR spectra were obtained using a Varian E-112 X-band spectrometer with a magnetic field center of 325.0 mT and a field sweep width of 20.0 mT. The semiquinone bound at the Q_i site was assayed from the antimycin-sensitive component by measuring the peak to trough amplitude of the g = 2.005 signal obtained at 100 K with a microwave power of 0.2 mW, with occupancy shown in arbitrary units.

^{1}H–^{14}N ESEEM spectra were identical with the spectra of unlabeled UQ-10 SQs measured in the isolated bc_1 complex,[20,21] thus confirming similar H-bond patterns, independent of isolation procedures, membrane location, or ^{13}C labeling. This similarity also shows that there is no significant contribution to the spectra from SQ species at catalytic sites outside the bc_1 complex.

Spectroscopic Properties. The ^{13}C hyperfine couplings in SQ_i were probed by HYSCORE experiments. Figure 3 (left) shows representative HYSCORE spectra for SQ_i in the

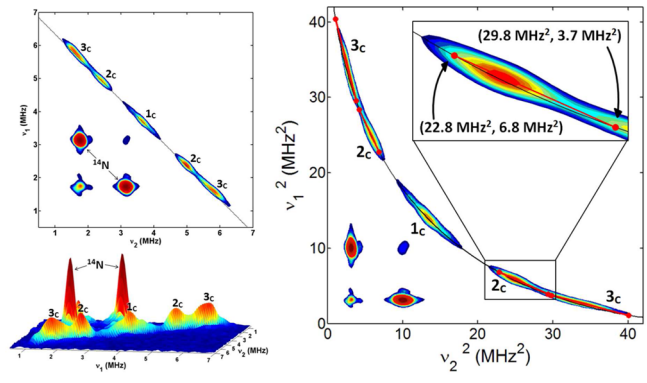

Figure 3. Contour (left, top) and stacked (left, bottom) HYSCORE spectra of SQ_i in the bc_1 complex [magnetic field of 343.0 mT, time between first and second pulses (τ) of 136 ns, and microwave frequency of 9.619 GHz]. Contour presentation of the HYSCORE spectra of SQ_i in $(\nu_1)^2$ vs $(\nu_2)^2$ coordinates (right). The curved line is defined by $|\nu_1 + \nu_2| = 2\nu_C$. The inset shows the linear regression fit for selected cross-peak $\mathbf{2}_C$. A graph showing the insert for the fitted ridge $\mathbf{3}_C$ is included in the Supporting Information.

dx.doi.org/10.1021/bi500654y | *Biochemistry* 2014, 53, 6022–6031

frequency interval from 0 to 7 MHz for both axes. The spectrum of SQ_i contains the lines from ^{14}N and ^{13}C nuclei. ^{14}N cross-peaks with coordinates (3.1, 1.7) MHz produced by N_ε of H217 were previously analyzed in detail.[20,21] Here we focus on the analysis of the ^{13}C lines. The ^{13}C cross-features are located along the antidiagonal, symmetrically relative to the diagonal point (ν_C, ν_C) where ν_C is ~3.7 MHz, in the applied magnetic field. Those include peak $\mathbf{1}_C$ with extended shoulders around the diagonal point (ν_C, ν_C) and two pairs of cross-peaks $\mathbf{2}_C$ and $\mathbf{3}_C$. Peak $\mathbf{1}_C$ has resolved shoulders with a splitting of ~1 MHz (see also Figure S3 of the Supporting Information). Cross-peaks $\mathbf{2}_C$ and $\mathbf{3}_C$ are partially overlapped but possess well-separated maxima at (5.0, 2.4) MHz ($\mathbf{2}_C$) and (5.9, 1.6) MHz ($\mathbf{3}_C$), which correspond to first-order estimated hyperfine couplings of 2.6 and 4.3 MHz, respectively.

Hyperfine tensors of the ^{13}C nuclei contributing to the spectrum of SQ_i can be obtained from the analysis of the contour line shape of the cross-peaks. An analytical estimate of the ^{13}C hyperfine tensors, i.e., a (isotropic coupling constant) and T (anisotropic coupling constant), was performed by plotting the HYSCORE spectrum in $(\nu_1)^2$ versus $(\nu_2)^2$ coordinates[41] (Figure 3, right). As a result, cross-peaks that are approximately axial appear as linear segments that can be fit to a linear regression. Intersection points of the linear fit with the line $|\nu_1 + \nu_2| = 2\nu_C$ define the principal values of the hyperfine tensor. There are two possible assignments to ($\nu_{\alpha\perp}$, $\nu_{\beta\perp}$) or ($\nu_{\alpha\parallel}$, $\nu_{\beta\parallel}$) for each crossing point and, consequently, two solutions, one for each assignment. Linear regression analysis of cross-peaks $\mathbf{2}_C$ and $\mathbf{3}_C$ and calculation of the tensors are discussed in the Supporting Information (Table S1 and Figure S2).

To choose between the two sets of axial tensors from the analysis of the ^{13}C HYSCORE plotted as $(\nu_1)^2$ versus $(\nu_2)^2$, the ^{13}C ridges for SQ_i were simulated with EasySpin.[39] Simulations were done starting from the squared-frequency analysis and then further optimized by adjusting the values and introducing rhombicity factor δ into the anisotropic hyperfine tensor $(-T(1 + \delta), -T(1 - \delta), 2T)$. Simulated spectra were found to be essentially independent of the relative Euler angles between the ^{13}C hyperfine tensors, possibly because of the low level of hyperfine anisotropy. Thus, calculations were performed without adjusting the Euler angles. Spectra for two possible tensors for cross-features $\mathbf{2}_C$ and $\mathbf{3}_C$ and their comparison with the experiments are provided in the Supporting Information (Table S2 and Figure S3).

Special comment is needed with regard to the analysis of feature $\mathbf{1}_C$. It did not fit well with a single set of a and T. This suggested that $\mathbf{1}_C$ results from a distribution of methoxy orientations, and therefore, a distribution of a and T may be necessary. However, even after an approximate distribution of hyperfine tensors had been implemented, the simulations were unable to match the spectrum, giving a simple featureless peak centered on the diagonal. As seen in the spectrum, peak $\mathbf{1}_C$ instead clearly has symmetrical shoulder features with a splitting of ~1.0 MHz. A reasonable fit for the $\mathbf{1}_C$ line shape was achieved using a two-state model. T is not expected to vary significantly from 0.5 MHz following the data listed in Table 2. Thus, it was fixed to that value, and spectra were simulated with two unique isotropic coupling constants a corresponding to two different methoxy orientations contributing to $\mathbf{1}_C$. Optimization of the rhombicity for $\mathbf{1}_C$ (which is fixed along with T for both methoxy orientations in the simulations), the actual values of the two a's, and the relative populations of the two states has given a surprisingly agreeable simulation when ~60% is due to a methoxy conformation giving a = 0.2 MHz and 40% for a = 1.1 MHz (Figure S3 of the Supporting Information). The final results of the simulations are summarized in Table 2 for comparison with the similar ^{13}C tensors for SQ_A and SQ_B in bacterial reaction centers.[31]

Table 2. ^{13}C Hyperfine Tensors Determined from the HYSCORE Spectral Simulations for SQ_i in Comparison with SQ_A and SQ_B

	^{13}C peak	a_{iso} (MHz)	T (MHz)
Q_i	$\mathbf{1}_C$	0.2 (60%) and 1.1 (40%)	0.5 (δ = 0.4)
	$\mathbf{2}_C$	2.5	0.5 (δ = 0.5)
	$\mathbf{3}_C$	−4.4	0.6 (δ = 0.3)
Q_A[a]	$\mathbf{1}_C$	0	0.4
	$\mathbf{2}_C$	1.3	0.5
	$\mathbf{3}_C$	−3.7	0.4
Q_B[a]	$\mathbf{1}_C$	1.5	0.4 (δ = 0.8)[b]
	$\mathbf{2}_C$	−3.8	0.4
	$\mathbf{3}_C$	4.6	0.5 (δ = 0.3)[b]

[a]From ref 31. [b]δ was reported incorrectly in ref 31 and has been corrected here.

DISCUSSION

Structural Considerations. High-resolution structures of mitochondrial (bovine, chicken, and yeast at ≥2.1 Å) and bacterial complexes (at ≥2.6 Å) show different configurations of the quinone species bound at the Q_i site,[16,26,27,30,42−44] but all have the same two residues close enough to the quinone to allow formation of either direct or H_2O-mediated H-bonds, H217 and D252 (in *Rb. sphaeroides* numbering). In a model structure,[21] N221 was positioned as a potential ligand to one of the methoxy O atoms, but the distance seen in crystallographic structures is not compatible with such a role (Figure 1). In the bovine mitochondrial complex (italic numbering), the corresponding residues are *H201* and *D228*, with N221 replaced by *S205*. However, we note that in relation to this discussion, the data from crystallographic structures relate to an unknown redox state of the Q_i site occupant. Also, the *B* factors of the occupant, even for the highest-resolution structures, show more disorder than the best defined regions, and there is considerable disagreement between different structures with respect to the configuration. Because of these ambiguities, interpretation with respect to semiquinone binding and selection of models for quantum calculation cannot be unequivocal. However, mutagenesis studies provided strong evidence of a functional role for each of these residues.[10,17−19]

DFT Computations of ^{13}C Tensors. For the selectively ^{13}C-labeled UQ-10 used here, three ^{13}C hyperfine couplings are expected corresponding to the two methoxy groups and the 5-CH_3 group carbon nuclei. The HYSCORE spectra of Figure 3 clearly illustrate these three ^{13}C features for SQ_i. Analysis of the spectra shows that for SQ_i one of these carbons has a small hyperfine coupling of ~0−1 MHz, whereas values with magnitudes of 2.5 and 4.4 MHz can be estimated for the other two. For the assignment of these measured tensors to the ^{13}C nuclei of the methyl or methoxy groups, it is necessary to compare with previous experimental results *in vitro* and *in vivo* or with values calculated using DFT approaches.

dx.doi.org/10.1021/bi500654y | *Biochemistry* 2014, 53, 6022−6031

The DFT computational approach extensively tested on the Q_A and Q_B sites in the bacterial reaction center from *Rb. sphaeroides*[45−47] has also been applied to the Q_i site. We have chosen to use the highest-resolution bovine mitochondrial structure available (PDB entry 1PP9 at ≥2.1 Å resolution)[26] as the basis for our model, although the bacterial structure (PDB entry 2QJY at ≥2.6 Å resolution)[16] might seem to be the obvious choice. The rationale for this choice is as follows. (i) The quantum chemical models contain only *D228* and *H201* as contributions from the protein, and these same side chains (*D252* and *H217*) contribute in the *Rb. sphaeroides* structures. (ii) Neither of the other potential ligands, *S205* in mitochondria or *N221* in *Rb. sphaeroides*, is within H-bonding distance of the quinone species in the structures. Other groups undoubtedly contribute to the site, but we have no justification for preferring the lower-resolution structure unless experimental data are available to show specific parameters that would affect the EPR data. We have analyzed two cases for the Q_i site of the bovine bc_1 complex structure (PDB entry 1PP9), with *H201* either deprotonated (a) or protonated (b) at N_δ (Figure S4 of the Supporting Information). Both models indicate that the COOH group of *D228* and the $N_\varepsilon H$ group of *H201* are hydrogen bonded to the carbonyls of the semiquinone. Geometry optimization of both models shows that when N_δ of *H201* is protonated, the proton from $N_\varepsilon H$ transfers to quinone O4 and the SQ is a neutral free radical with its OH group acting as a donor of a hydrogen bond to N_ε of *H201*. For the deprotonated N_δ model, the SQ is an anion radical with both its O1 and O4 atoms accepting hydrogen bonds from *D228* and *H201*, respectively. Previous experimental data for H-bond protons and N_ε[20−22] are more consistent with the anion radical and rule out the neutral radical. The DFT-calculated ^{13}C hyperfine couplings for the anion radical model are listed in Table 3, where we compare these with the experimental determinations. The DFT-calculated values strongly support the assignment of the largest-magnitude 4.4 MHz value to the 5-CH_3 carbon, the 2.5 MHz value to the 3-methoxy carbon, and the smaller-magnitude 0.2 or 1.0 MHz value to the 2-methoxy carbon.

Table 3. Calculated ^{13}C, Isotropic Constant (a), and Anisotropic Hyperfine Tensor Components (T_{nn}) (in megahertz) for the Anion Radical Model of SQ_i[a]

position		a
$^{13}C-CH_3$ (5)	0.8 (T_{11})	−4.8 (|4.4|)
	−0.4 (T_{22})	
	−0.4 (T_{33})	
$^{13}C-CH_3O$ (3)	0.8 (T_{11})	2.0 (|2.5|)
	−0.2 (T_{22})	
	−0.6 (T_{33})	
$^{13}C-CH_3O$ (2)	0.6 (T_{11})	0.5 (|0.2|, |1.0|)
	−0.1 (T_{22})	
	−0.6 (T_{33})	

[a]The magnitudes of the experimental isotropic hyperfine couplings are given in parentheses.

Spin populations calculated previously for the ubisemiquinones in model systems (Q_A and Q_B quinone sites[31] and the high-affinity Q_H site of cytochrome bo_3 ubiquinol oxidase and its D75H mutant[5,48]) are shown in Table 4. The last row contains spin populations for the anion radical in the Q_i site. Our assignment of the largest hyperfine coupling to the 5-CH_3 group in SQ_i is also consistent with experimental and calculated isotropic hyperfine couplings (Table 5) for the ubisemiquinones from Table 4.

Table 4. Mülliken Spin Populations in Selected SQs

semiquinone	C2	C3	C5
SQ_A[a]	0.11	−0.01	0.05
SQ_B[a]	0.09	0.03	0.07
SQ_{M1}[a,c]	0.07	0.07	0.09
SQ_{M2}[a,c]	0.11	0.00	0.07
SQ_H[b]	−0.02	0.16	0.14
SQ_H (D75H)[b]	0.00	0.16	0.13
SQ_i	0.06	0.05	0.11

[a]From ref 31. [b]From ref 48. [c]SQ_{M1}, 6-methyl-UQ with four H_2O molecules; SQ_{M2}, 6-methyl-UQ with one H_2O (see Figure S5 of the Supporting Information).

Table 5. Comparison of Experimental and Calculated ^{13}C Methyl (5′) Isotropic Couplings in SQs

semiquinone	$a_{exp}(^{13}C)$ (MHz)	$a_{calc}(^{13}C)$ (MHz)
SQ_A	−3.6[a]	−2.9[a]
SQ_B	−4.0[a]	−3.5[a]
$(UQ\text{-}10)^-$	|4.0|[b]	−3.0[a]
SQ_H	−6.1[c]	−5.3[d]
SQ_H (D75H)	−4.7[c]	−4.4[d]
SQ_i	−4.4	−4.8

[a]From ref 31. [b]From ref 49. [c]From ref 5. [d]From ref 48.

The spin populations in Table 4 demonstrate the asymmetry of the spin density distribution in different SQs resulting from different interactions with their protein environment. Spin densities obtained for SQ_H arise from stronger hydrogen bonding with O1. In contrast, the opposite asymmetry of spin density distribution in the Q_A site suggests stronger hydrogen bonding at O4. The asymmetry in spin density distribution observed for the SQ_i radical might indicate that a slightly stronger hydrogen bond is formed at O1 with D252. A notable peculiarity of the unpaired spin density distribution for SQ_i is the similarity of values for the spin populations on C2 (0.06) and C3 (0.05). This is in contrast with the Q_A and Q_B sites where the C2 population is much larger than C3 or with the Q_H site where the opposite relationship occurs.

As shown previously, the ^{13}C isotropic hyperfine coupling of the methoxy group will be proportional to the π(p) spin population of the corresponding ring carbon and the dihedral angle of the methoxy CO bond with respect to the SQ ring plane.[31] The unpaired spin density giving rise to the ^{13}C isotropic hyperfine coupling for the methoxy group carbon atom arises from a combination of spin polarization and hyperconjugation. When the methoxy group is held in the ring plane, hyperconjugation is expected to be zero and small negative hyperfine couplings are expected for in-plane or near to in-plane orientations, due to spin polarization by the methoxy oxygen spin density. As the methoxy orientation is moved progressively out of plane, a positive contribution from hyperconjugation with the ring carbon π(p) spin density arises.[31] The agreement with experiments observed in Table 3 for the geometry-optimized isolated SQ_i model (starting from the crystal structure coordinates) suggests that the methoxy

dx.doi.org/10.1021/bi500654y | *Biochemistry* 2014, 53, 6022−6031

groups in the Q_i site are close to the minimal energy conformation of an isolated SQ. The conformations for the minimal energy model are 3-methoxy (CM2−O2−C2−C1) = −68° and 2-methoxy (CM3−O3−C3−C4) = 56°. This is in contrast to the Q_A and Q_B site semiquinones in bacterial photosynthetic reaction centers, which deviate significantly from the optimal angles for an isolated model.

Influence of the Protein Environment on Methoxy Conformations. HYSCORE spectra of the SQ in the Q_A, Q_B, and Q_i sites resolve all three cross-peaks from the three ^{13}C site-specifically labeled nuclei in the SQ structure, thus suggesting significant constraints on the methoxy group conformation by the protein environment. The 2-methoxy groups in SQ_A and SQ_B were shown to give rise to quite distinct ^{13}C isotropic hyperfine couplings, with the magnitude of SQ_B exceeding that of SQ_A (Table 2). The larger value for SQ_B could be qualitatively explained by a more out-of-plane orientation of the 2-methoxy group compared with SQ_A. DFT calculations demonstrated a strong dependence of the electron affinity of the quinone on the methoxy dihedral angles,[31] and the higher redox potential of the Q_B ubiquinone was rationalized on this basis. A similar comparative analysis for the 3-methoxy orientation was however precluded by the negligible unpaired spin density on the adjusted C3 atom in SQ_A (Table 4). In contrast to SQ_A and SQ_B, direct computation of the SQ_i optimized structure and distribution of the unpaired spin density allows us to assign the observed ^{13}C couplings to particular substituents and gives an estimated conformation of 3-methoxy that possesses a larger isotropic coupling (and larger deviation) than 2-methoxy. On the other hand, this approach leaves open the interpretation of the complex line shape of peak $\mathbf{1}_C$ assigned to the 2-methoxy group and suggests a behavior more complex than a single conformation with a small strain. Analysis of the bovine mitochondrial complex (PDB entry 1PP9) shows a different conformation of the methoxy group for the quinone in the Q_i site that may correlate with the two-conformation model giving a best fit of $\mathbf{1}_C$ peaks with the simulated spectra. This structural difference, however, was not found in lower-resolution bacterial structures.

In contrast to the spectra in proteins, the HYSCORE spectrum for the ^{13}C methyl, methoxy-labeled anion radical of UQ-10 in alcohol consists of two broad cross-peaks extending along the antidiagonal (Figure S6 of the Supporting Information) and does not show significant intensity around the diagonal point. This spectrum may indicate substantial discrete line widths of three individual couplings contributing to these cross-peaks. In addition, the similarity between the spin density on C2 and C3 for the anion radical (model SQ_{M1} in Table 4) suggests that its spin density distribution is described well by the model and indicates a significant average deviation from the in-plane configuration for both methoxy groups in an alcohol solution. The spin density at C2 and C3 in SQ_i is also similar, but the spectra are quite different, suggesting that a dynamic situation in solution is replaced by a more constrained configuration in the protein environment.

For the Q_A and Q_B sites, it has been suggested that modification of the methoxy orientation fine-tunes the redox potentials to ensure the transfer of an electron from Q_A to Q_B. However, the operational ranges at both Q_A and Q_B sites ($E_{m,7}$ values of −100 and 0 mV, respectively) are at redox potentials much lower than that of the Q pool ($E_{m,7} \sim 90$ mV), while both the Q_i site ($E_{m,7} \sim 150$ mV) and the Q_o site ($E_{m,7} \sim 120$ mV) function at a higher potential.[8,53] This substantial difference must be considered in discussing any such control. The higher redox potential for Q_i would at least qualitatively be in accord with having methoxy groups near the minimal energy conformations for the SQ form. This stabilizes the semiquinone, increasing both the electron affinity and the redox potential. However, the high potential for the Q/QH_2 couple at both these Q_i and Q_o sites is achieved through preferential binding of QH_2. Although both sites operate in the high-potential range, their mechanism and function are very different. The difference in function comes in part from the wide difference in SQ stability and in part from mechanistic differences. The higher stability of SQ_i allows it to function as an intermediate, storing the first electron in a two-electron gate mechanism. This stability might reflect the minimal energy configuration but certainly also reflects the two H-bonds shown by our earlier ESEEM work.[20−22] In the bifurcated reaction at the Q_o site,[53] the very unstable SQ_o allows a thermodynamic coupling between two electron transfer pathways, so that the work derived from oxidation of QH_2 to SQ by the high-potential chain (ISP, heme c_1, and cyt c_2) generates a strong reductant in the Q/SQ couple to drive reduction at the Q_i site, and maintenance of the proton gradient by electrogenic electron transfer across the membrane. Clearly, factors other than methoxy orientation are in play in the mechanisms of both sites.

The apparent influence of the protein environment on the conformation of the methoxy groups in each particular case suggests that the role of the methoxy conformations in the Q_i site of the bc_1 complex could be better understood from experiments with Q_i site mutants. A strategy exploiting mutagenesis in the context of the synergy between spectroscopy and specific isotopic labeling made possible with auxotrophic strains, and used with great success in studies of the SQ_H species of the bo_3 oxidase of *E. coli*,[5,48] can now be applied to the bc_1 complex, where the richness of structural information and kinetic studies opens wider horizons.

Mechanism of Formation of SQ at the Q_i Site. In earlier models, formation of the SQ was considered in the context of the disproportionation equilibria, determined by $K_S = ([SQ]^2)/([Q][QH_2])$. An anomalous feature was the low occupancy (<0.5/heme b_H), accounted for either in terms of a dimeric model,[14] in which only one monomer could be occupied at a time, or by quenching of the EPR signal by ferriheme b_H in a fraction of the centers,[15,50] or by invoking limitations arising from the dissociation state of a protein group.[15] A third class of mechanism involved the "cyt *b*-150" phenomena.[19,51] Redox titration of heme b_H in the presence of antimycin shows a component usually analyzed as a single species with an $E_{m,7}$ of ∼40 mV. However, in the absence of antimycin, the titration is biphasic, showing the same overall amplitude, but with a fraction (dependent on pH) titrating at $E_{m,7} \sim 150$ mV. Addition of antimycin induced a loss of this component to give an antimycin-induced oxidation (see ref 52 for discussion). The pH dependence of the 150 mV component correlated well with the pH dependence of SQ formation, suggesting participation of heme b_H in the formation of SQ through reversal of the normal forward chemistry. As structures became available, and more detailed spectroscopic observation addressed the binding of the SQ more directly, additional complicating features were identified. In particular, as discussed in ref 20, it seems probable that the pattern of H-bonding with the protein must change with the redox state of the quinone species involved, and with the dissociation state of H217 and D252. The line width of the

dx.doi.org/10.1021/bi500654y | *Biochemistry* 2014, 53, 6022−6031

SQ signal indicates the anionic semiquinone over a wide range of pH, so the pH dependence has to be attributed to dissociable group(s) of the protein rather than of the SQ_i^-.[15] These questions have not recently been revisited, and detailed discussion in the present context would be out of place. However, because the quantum chemical calculations suggest that the anionic semiquinone is associated with a protonated H217, it seems likely that this residue is the dissociable group needed to explain the pH dependence of SQ stability[15] and identified in this role in ref 20. The other direct ligand included in the quantum chemical calculations is D252. It is likely that the pK_a of this group in some configurations (for example, a vacant site) would be influenced by interaction with K251, not yet included in the model. In previous reports of the effects of mutation at N221,[10,22] we had discounted any importance of H-bonding because the N221P strain showed kinetic behavior and thermodynamic properties similar to those of the wild type. Although we could not exclude a weak interaction of N221 with the methoxy O on the basis of ^1H, ^2H, ^{14}N, or ^{15}N proton spin interactions,[20−22] the high activity of the N221P strain and the similarity of the kinetic behavior to that of the wild type seemed to argue strongly against any H-bonding interaction. More recent experiments have failed to reproduce this result. Unfortunately, the original N221P strain was lost, but analysis of cells recovered from frozen stocks of chromatophore preparations used in previous experiments showed the wild-type sequence. We therefore believe our earlier results represent a wild-type strain obtained by either reversion or contamination. We have reconstructed an authentic N221P strain, but all attempts to grow this strain under anaerobic photosynthetic conditions, which require an active bc_1 complex, have failed. The failure of the authentic N221P strain to grow would then indicate an important H-bonding role for the native asparagine side chain, supported by the low rates seen in N221I mutants.[22] This necessitates a revision of our earlier conclusions, with respect to both a general H-bonding role and a more specific side chain-dependent interaction. In structures, N221 is too distant to form a direct H-bond through the side chain to the methoxy O (Figure 1 and Table 1), but this would be pertinent to the data presented here only if the X-ray beam had induced reduction of the SQ. The side chain is involved in a network of H-bonded groups that includes waters and the heme propionates, and MD simulations (see ref 53) suggest additional waters that might provide a proton channel to the N phase. The strong inhibition of transfer of an electron from heme b_H to the Q_i site upon mutation at N221 could then indicate that the equilibration of the heme propionates, and possibly of H111 and the SQ, with the pH of the N phase is important in facilitating this electron transfer step. This brings up the question of how heme b_H is involved in the formation of the SQ. The "cyt *b*-150" model had suggested that the SQ is formed via reversal of the forward reaction:

$$\text{heme } b_H \text{ (vacant)} + QH_{2(\text{pool})} \rightleftharpoons \text{heme } b_H{\cdot}QH_2 \rightleftharpoons \text{heme } b^-_H{\cdot}SQ^-(H^+) + H^+$$

$$\text{heme } b^-_H{\cdot}SQ^-(H^+) + \text{antimycin (via reversal of above)} \downarrow \text{heme } b_H{\cdot}\text{antimycin} + QH_2$$

These reactions account well for the "cyt *b*-150" phenomena, and the oxidation of heme b^-_H induced upon addition of antimycin,[19,51] but a simple thermodynamic model does not explain the SQ occupancy or the shape of the titration curve (which in the model was pH-dependent but experimentally shows the same shape at all pH values). No detailed model including specification of the dissociable groups involved in the equilibration of protons with the "visible" reactants is yet available.

A more detailed examination of these different possibilities must await further work on characterization of strains with mutations at key residues involved in liganding the SQ or protonic equilibration of the reaction components, more detailed MD and quantum chemical models, and spectroscopic studies exploiting specific isotopic labeling that will be possible with extensions of this work to other auxotrophic strains.

CONCLUSION

Specific isotopic labeling at the residue or substituent level extends the scope of several important spectroscopic approaches to structure at the atomistic level. Here we demonstrate isotopic labeling of the ring substituents of ubiquinone, achieved through construction of a methionine auxotroph in *Rb. sphaeroides* strain BC17, and used to explore the question of electronic structure and geometry of substituents at the Q_i site of the bc_1 complex. This topic has been controversial, with different results reported from crystallography and from pulsed EPR studies in mitochondrial and bacterial complexes. We extend our studies of the complex in *Rb. sphaeroides* by isotopic labeling of the methyl and methoxy substituents of the ubiquinone ring using ^{13}C and determination of the interaction of the nuclear spins with the electron spin of the semiquinone generated *in situ* in the complex in its membrane environment. By using HYSCORE spectroscopy, we have measured the isotropic and anisotropic spin couplings to allow comparison with properties previously estimated in the Q_A and Q_B sites of the bacterial reaction center, and the Q_H site of the cyt bo_3 oxidase of *E. coli*. Differences between these sites, and the strong dependence of isotropic couplings on the dihedral angles of the substituents, allow an exploration of the orientation of the semiquinone methoxy groups in the catalytic site. The protocol used in generation of the methionine auxotroph is applicable more generally and, because it introduces a gene deletion using a suicide plasmid, can be applied repeatedly. In particular, because auxotrophy often will require deletion of a single gene, it is convenient when a highly engineered background has been developed for mutational engineering in the context of a specific protein, because previous manipulations are undisturbed. In our case, construction of an auxotroph in the BC17 strain allows conclusions from the spectroscopic studies to be directly compared with experimental data derived from *in situ* assays of function through kinetic spectrophotometry using an extensive collection of mutant strains.

ASSOCIATED CONTENT

Supporting Information

Relevant methodological details and Figures S1−S6. This material is available free of charge via the Internet at http://pubs.acs.org.

AUTHOR INFORMATION

Corresponding Authors

*E-mail: crofts@illinois.edu. Phone: (217) 333-2043.
*E-mail: dikanov@illinois.edu. Phone: (217) 300-2209.

*E-mail: patrick.omalley@manchester.ac.uk. Phone: 00441612004536.

Present Address

[#]Departamento de Química Inorgânica, Instituto de Química, Universidade Federal Fluminense, Campus do Valonguinho, Centro, Niterói, RJ, CEP: 24020-141, Brazil

Funding

This research was supported by Grants DE-FG02-08ER15960 (S.A.D.) and DE-FG02-87ER13716 (R.B.G.) from the Chemical Sciences, Geosciences and Biosciences Division, Office of Basic Energy Sciences, Office of Sciences, U.S. Department of Energy, National Institutes of Health (NIH) Grant GM062954 (S.A.D.), and National Center for Research Resources Grants S10-RR15878 and S10-RR025438 for pulsed EPR instrumentation. P.J.O. acknowledges the use of computer resources granted by the EPSRC UK national service for computational chemistry software (NSCCS). A.T.T. gratefully acknowledges support as a NIH trainee of the Molecular Biophysics Training Program (5T32-GM008276). W.B. De Almeida would like to thank FAPEMIG (Fundação de Amparo a Pesquisa no Estado de Minas Gerais) for financial support during his stay at The University of Manchester, UK, and CNPq (Conselho Nacional de Desenvolvimento Científico e Tecnológico) for a research grant. We also thank the University of Manchester Computer Share Facilities (CSF) for providing computational resources to develop this work.

Notes

The authors declare no competing financial interest.

■ ACKNOWLEDGMENTS

We thank Professors Sam Kaplan, Ronald MacKenzie, and Jesus Eraso for making available their set of auxotrophic strains and for advice on engineering gene deletions.

■ ABBREVIATIONS

2D, two-dimensional; CW, continuous-wave; DFT, density functional theory; B3LYP, Becke3 Lee−Yang−Parr; SQ, semiquinone; EPR, electron paramagnetic resonance; ESEEM, electron spin echo envelope modulation; HYSCORE, hyperfine sublevel correlation; UQ-10, ubiquinone-10.

■ REFERENCES

(1) Nicholls, D. G., and Ferguson, S. J. (2013) *Bioenergetics*, 4th ed., Academic Press, Elsevier, Amsterdam.

(2) Mitchell, P. (1966) *Chemiosmotic Coupling in Oxidative and Photosynthetic Phosphorylation*, Glynn Research Ltd., Bodmin, Cornwall, U.K.

(3) Mitchell, P. (1968) *Chemiosmotic Coupling and Energy Transduction*, Glynn Research Ltd., Bodmin, Cornwall, U.K.

(4) Lin, I.-J., Chen, Y., Fee, J. A., Song, J., Westler, W. M., and Markley, J. L. (2006) Rieske Protein from *Thermus thermophilus*: ^{15}N NMR Titration Study Demonstrates the Role of Iron-Ligated Histidines in the pH Dependence of the Reduction Potential. *J. Am. Chem. Soc. 128*, 10672−10673.

(5) Lin, M. T., Shubin, A. A., Samoilova, R. I., Narasimhulu, K. V., Baldansuren, A., Gennis, R. B., and Dikanov, S. A. (2011) Exploring by pulsed EPR the electronic structure of ubisemiquinone bound at the Q_H site of cytochrome bo_3 from *Escherichia coli* with *in vivo* ^{13}C-labeled methyl and methoxy substituents. *J. Biol. Chem. 286*, 10105−10114.

(6) Mackenzie, C., Simmons, A. E., and Kaplan, S. (1999) Multiple chromosomes in bacteria: The Yin and Yang of *trp* gene localization in *Rhodobacter sphaeroides* 2.4.1. *Genetics 153*, 525−538.

(7) Cramer, W. A., Zhang, H., Yan, J., Kurisu, G., and Smith, J. L. (2004) Evolution of photosynthesis: Time-independent structure of the cytochrome b_6f complex. *Biochemistry 43*, 5921−5929.

(8) Crofts, A. R. (2004) The Q-cycle: A personal perspective. *Photosynth. Res. 80*, 223−243.

(9) Kramer, D. M., Nitschke, W., and Cooley, J. W. (2009) The cytochrome bc_1 and related *bc* complexes: The Rieske/cytochrome *b* complex as the functional core of a central electron/ proton transfer complex. *The Purple Phototrophic Bacteria* (Hunter, C. N., Daldal, F., Thurnauer, M. C., and Beatty, J. T., Eds.) pp 451−473, Springer Science, New York.

(10) Crofts, A. R., Holland, J. T., Victoria, D., Kolling, D. R., Dikanov, S. A., Gilberth, R., Lhee, S., Kuras, R., and Kuras, M. G. (2008) The Q-cycle reviewed: How well does a monomeric mechanism of the bc_1 complex account for the function of a dimeric complex? *Biochim. Biophys. Acta 1777*, 1001−1019.

(11) Mitchell, P. (1976) Possible molecular mechanisms of the protonmotive function of cytochrome systems. *J. Theor. Biol. 62*, 327−367.

(12) Trumpower, B. L. (1981) Function of the iron-sulfur protein of the cytochrome b-c_1 segment of the respiratory chain. *Biochim. Biophys. Acta 639*, 129−155.

(13) Crofts, A. R., Meinhardt, S. W., Jones, K. R., and Snozzi, M. (1983) The role of the quinone pool in the cyclic electron-transfer chain of *Rhodopseudomonas sphaeroides*: A modified Q-cycle mechanism. *Biochim. Biophys. Acta 723*, 202−218.

(14) de Vries, S., Berden, J. A., and Slater, E. C. (1982) Oxidation-reduction properties of an antimycin-sensitive semiquinone anion bound to QH_2:cytochrome *c* oxidoreductase. *Function of Quinones in Energy Conserving Systems* (Trumpower, B. L., Ed.) pp 235−246, Academic Press, New York.

(15) Robertson, D. E., Prince, R. C., Bowyer, J. R., Matsuura, K., Dutton, P. L., and Ohnishi, T. (1984) Thermodynamic properties of the semiquinone and its binding site in the ubiquinol: Cytochrome *c* (c_2) oxidoreductase of respiratory and photosynthetic systems. *J. Biol. Chem. 259*, 1758−1763.

(16) Esser, L., Elberry, M., Zhou, F., Yu, C.-A., Yu, L., and Xia, D. (2008) Inhibitor complexed structures of the cytochrome bc_1 complex from the photosynthetic bacterium *Rhodobacter sphaeroides*. *J. Biol. Chem. 283*, 2846−2857.

(17) Gray, K. A., Dutton, P. L., and Daldal, F. (1994) Requirement of histidine-217 for ubiquinone reductase activity (Q_i-site) in the cytochrome-bc_1 complex. *Biochemistry 33*, 723−733.

(18) Brasseur, G., Sami Saribas, A., and Daldal, F. (1996) A compilation of mutations located in the cytochrome *b* subunit of the bacterial and mitochondrial bc_1 complex. *Biochim. Biophys. Acta 1275*, 61−69.

(19) Hacker, B., Barquera, B., Crofts, A. R., and Gennis, R. B. (1993) Characterization of mutations in the cytochrome *b* subunit of the bc_1 complex of *Rhodobacter sphaeroides* that affect the quinone reductase site (Q_c). *Biochemistry 32*, 4403−4410.

(20) Kolling, D. R. J., Samoilova, R. I., Holland, J. T., Berry, E. A., Dikanov, S. A., and Crofts, A. R. (2003) Exploration of ligands to the Q_i-site semiquinone in the bc_1 complex using high resolution EPR. *J. Biol. Chem. 278*, 39747−39754.

(21) Dikanov, S. A., Samoilova, R. I., Kolling, D. R. J., Holland, J. T., and Crofts, A. R. (2004) Hydrogen bonds involved in binding the Q_i-site semiquinone in the bc_1 complex, identified through deuterium exchange using pulsed EPR. *J. Biol. Chem. 279*, 15814−15823.

(22) Dikanov, S. A., Holland, J. T., Endeward, B., Kolling, D. R., Samoilova, R. I., Prisner, T. F., and Crofts, A. R. (2007) Hydrogen bonds between nitrogen donors and the semiquinone in the Q_i-site of the bc_1 complex. *J. Biol. Chem. 282*, 25831−25841.

(23) MacMillan, F., Lange, C., Bawn, M., and Hunte, C. (2010) Resolving the EPR spectra in the cytochrome bc_1 complex from *Saccharomyces cerevisiae*. *Appl. Magn. Reson. 37*, 305−316.

(24) Salerno, J. C., Osgood, M., Liu, Y., Taylor, H., and Scholes, C. P. (1990) Electron nuclear double resonance (ENDOR) of the Q_c-ubiSQ

radical in the mitochondrial electron transport chain. *Biochemistry 29*, 6987−6993.
(25) Gao, X., Wen, X., Esser, L., Quinn, B., Yu, L., Yu, C.-A., and Xia, D. (2003) Structural basis for the quinone reduction in the bc_1 complex: A comparative analysis of crystal structures of mitochondrial cytochrome bc_1 with bound substrate and inhibitors at the Q_i site. *Biochemistry 42*, 9067−9080.
(26) Huang, L. S., Cobessi, D., Tung, E. Y., and Berry, E. A. (2005) Binding of the respiratory chain inhibitor antimycin to the mitochondrial bc_1 complex: A new crystal structure reveals an altered intramolecular hydrogen-bonding pattern. *J. Mol. Biol. 351*, 573−597.
(27) Hunte, C., Koepke, J., Lange, C., Roßmanith, T., and Michel, H. (2000) Structure at 2.3 Å resolution of the cytochrome bc_1 complex from the yeast *Saccharomyces cerevisiae* co-crystallized with an antibody F_v fragment. *Structure 8*, 669−684.
(28) Lange, C., Nett, J. H., Trumpower, B. L., and Hunte, C. (2001) Specific roles of protein-phospholipid interactions in the yeast bc_1 complex structure. *EMBO J. 23*, 6591−6600.
(29) Palsdottir, H., Lojero, C. G., Trumpower, B. L., and Hunte, C. (2003) Structure of the yeast cytochrome bc_1 complex with a hydroxyquinone anion Q_o site inhibitor bound. *J. Biol. Chem. 278*, 31303−31311.
(30) Zhang, Z., Huang, L.-S., Shulmeister, V. M., Chi, Y.-I., Kim, K.-K., Hung, L.-W., Crofts, A. R., Berry, E. A., and Kim, S.-H. (1998) Electron transfer by domain movement in cytochrome bc_1. *Nature 392*, 677−684.
(31) Taguchi, A. T., O'Malley, P. J., Wraight, C. A., and Dikanov, S. A. (2013) Conformational differences between the methoxy groups of Q_A and Q_B site ubisemiquinones in bacterial reaction centers: A key role for methoxy group orientation in modulating ubiquinone redox potential. *Biochemistry 52*, 4648−4655.
(32) Eraso, J. M., and Kaplan, S. (2002) Redox flow as an instrument of gene regulation. *Methods Enzymol. 348*, 216−229.
(33) Lenz, O., Schwartz, J., Eitinger, M., and Friedrich, B. (1994) The *Alcaligenes eutrophus* H16 hoxX gene participates in hydrogenase regulation. *J. Bacteriol. 176*, 4385−4393.
(34) Yun, C.-H., Beci, R., Crofts, A. R., Kaplan, S., and Gennis, R. B. (1990) Cloning and DNA sequencing of the *fbc* operon encoding the cytochrome bc_1 complex from *Rb. sphaeroides*: Characterization of *fbc* deletion mutants, and complementation by a site-specific mutational variant. *Eur. J. Biochem. 194*, 399−411.
(35) Donohue, T. J., McEwan, A. G., Van Doren, S., Crofts, A. R., and Kaplan, S. (1988) Phenotypic and genetic characterization of cytochrome c_2 deficient mutants of *Rhodobacter sphaeroides*. *Biochemistry 27*, 1918−1925.
(36) Bowyer, J. R., Tierney, G. V., and Crofts, A. R. (1979) Secondary Electron Transfer in Chromatophores of *Rhodopseudomonas capsulata* A1a pho$^-$: Binary Oscillations. *FEBS Lett. 101*, 201−206.
(37) Crofts, A. R., Guergova-Kuras, M., and Hong, S. (1998) Chromatophore heterogeneity explains effects previously attributed to supercomplexes. *Photosynth. Res. 55*, 357−362.
(38) Höfer, P., Grupp, A., Nebenführ, H., and Mehring, M. (1986) Hyperfine sublevel correlation (HYSCORE) spectrocopy: A 2D ESR investigation of the squaric acid radical. *Chem. Phys. Lett. 132*, 279−282.
(39) Stoll, S., and Britt, R. D. (2009) General and efficient simulation of pulse EPR spectra. *Phys. Chem. Chem. Phys. 11*, 6614−6625.
(40) Frisch, M. J., Trucks, G. W., Schlegel, H. B., Scuseria, G. E., Robb, M. A., Cheeseman, J. R., Scalmani, G., Barone, V., Mennucci, B., Petersson, G. A., Nakatsuji, H., Caricato, M., Li, X., Hratchian, H. P., Izmaylov, A. F., Bloino, J., Zheng, G., Sonnenberg, J. L., Hada, M., Ehara, M., Toyota, K., Fukuda, R., Hasegawa, J., Ishida, M., Nakajima, T., Honda, Y., Kitao, O., Nakai, H., Vreven, T., Montgomery, J. A., Jr., Peralta, J. E., Ogliaro, F., Bearpark, M., Heyd, J. J., Brothers, E., Kudin, K. N., Staroverov, V. N., Kobayashi, R., Normand, J., Raghavachari, K., Rendell, A., Burant, J. C., Iyengar, S. S., Tomasi, J., Cossi, M., Rega, N., Millam, J. M., Klene, M., Knox, J. E., Cross, J. B., Bakken, V., Adamo, C., Jaramillo, J., Gomperts, R., Stratmann, R. E., Yazyev, O., Austin, A. J., Cammi, R., Pomelli, C., Ochterski, J. W., Martin, R. L., Morokuma, K., Zakrzewski, V. G., Voth, G. A., Salvador, P., Dannenberg, J. J., Dapprich, S., Daniels, A. D., Farkas, Ö., Foresman, J. B., Ortiz, J. V., Cioslowski, J., and Fox, D. J. (2009) *Gaussian 09*, revision A.1, Gaussian, Inc., Wallingford, CT.
(41) Dikanov, S. A., and Bowman, M. K. (1995) Cross-peak lineshape of two-dimensional ESEEM spectra in disordered $S = 1/2$, $I = 1/2$ spin system. *J. Magn. Reson., Ser. A 116*, 125−128.
(42) Xia, D., Yu, C.-A., Kim, H., Xia, J.-Z., Kachurin, A. M., Zhang, L., Yu, L., and Deisenhofer, J. (1997) Crystal structure of the cytochrome bc_1 complex from bovine heart mitochondria. *Science 277*, 60−66.
(43) Iwata, S., Lee, J. W., Okada, K., Lee, J. K., Iwata, M., Rasmussen, B., Link, T. A., Ramaswamy, S., and Jap, B. K. (1998) Complete structure of the 11-subunit bovine mitochondrial cytochrome bc_1 complex. *Science 281*, 64−71.
(44) Berry, E. A., Huang, L.-S., Saechao, L. K., Pon, N. G., Valkova-Valchanova, M., and Daldal, F. (2004) X-ray structure of *Rhodobacter capsulatus* cytochrome bc_1: Comparison with its mitochondrial and chloroplast counterparts. *Photosynth. Res. 81*, 251−275.
(45) Lin, T.-J., and O'Malley, P. J. (2008) An ONIOM study of the Q_A site semiquinone in the *Rhodobacter sphaeroides* photosynthetic reaction centre. *THEOCHEM 870*, 31−35.
(46) Martin, E., Samoilova, R. I., Narasimhulu, K. V., Lin, T.-J., O'Malley, P. J., Wraight, C. A., and Dikanov, S. A. (2011) Hydrogen bonding and spin density distribution in the Q_B semiquinone of bacterial reaction centers and comparison with the Q_A site. *J. Am. Chem. Soc. 133*, 5525−5537.
(47) Martin, E., Baldansuren, A., Lin, T.-J., Samoilova, R. I., Wraight, C. A., Dikanov, S. A., and O'Malley, P. J. (2012) Hydrogen bonding between the Q_B site ubisemiquinone and Ser-L223 in the bacterial reaction center: A combined spectroscopic and computational perspective. *Biochemistry 51*, 9086−9093.
(48) Lin, M. T., Baldansuren, A., Hart, R., Samoilova, R. I., Narasimhulu, K. V., Yap, L.-L., Choi, S. K., O'Malley, P. J., Gennis, R. B., and Dikanov, S. A. (2012) Interactions of intermediate semiquinone with surrounding protein residues at the Q_H site of the wild-type and D75H mutant cytochrome bo_3 from *Escherichia coli*. *Biochemistry 51*, 3827−3838.
(49) Samoilova, R. I., Gritsan, N. P., Hoff, A. J., van Liemt, W. B. S., Lugtenburg, J., Spoyalov, A. P., and Tsvetkov, Yu. D. (1995) ENDOR and EPR studies of highly isotopically ^{13}C-enriched ubiquinone radicals. Part 2. *J. Chem. Soc., Perkin Trans. 2*, 2063−2068.
(50) de la Rosa, F. F., and Palmer, G. (1983) Reductive titration of CoQ-depleted Complex III from baker's yeast: Evidence for an exchange-coupled complex between $QH^\bullet$ and low-spin ferricytochrome *b*. *FEBS Lett. 163*, 140−143.
(51) Meinhardt, S. W., and Crofts, A. R. (1984) A new effect of antimycin on the *b*-cytochromes of *Rps. sphaeroides*. In *Advances in Photosynthesis Research* (Sybesma, C., Ed.) Martinus Nijhoff/Dr. W. Junk Publishers, The Hague, 1984; pp 649−652.
(52) Crofts, A. R. (2004) The cytochrome bc_1 complex: Function in the context of structure. *Annu. Rev. Physiol. 66*, 689−733.
(53) Crofts, A. R., Hong, S., Wilson, C., Burton, R., Victoria, D., Harrison, C., and Schulten, K. (2013) The mechanism of ubihydroquinone oxidation at the Q_o-site of the cytochrome bc_1 complex. *Biochim. Biophys. Acta 1827*, 1362−1377.